J Mater Sci (2006) 41:7954–7963
DOI 10.1007/s10853-006-0866-1

The effect of dissolved titanium on the primary α-Al grain and globule size in the conventional and semi-solid casting of 356 Al–Si Alloy

Shahrooz Nafisi · Reza Ghomashchi

Received: 15 July 2005 / Accepted: 15 November 2005 / Published online: 2 November 2006

Abstract The chemistry of molten alloy plays an important role on grain refining. Small addition of alloying elements reduces the grain size of the as-solidified structures to some degree depending on the alloy efficiency. The effect of dissolved Ti has been studied on the microstructure of Al–Si foundry alloys cast conventionally and by semi-solid casting routes. It is shown that Ti in solution could restrict the grains and globules size in both processes. A parallel plate compression test machine was employed to study the effect of dissolved Ti on the rheological behavior of the billets. It was confirmed billets with higher dissolved Ti-content have superior flow.

Introduction

The fact that solute elements in aluminum alloys have beneficial effects in reducing the grain size and improving mechanical properties of as-cast products goes back to Kissling and Wallace's work in 1963 [1]. It is generally believed that small addition of alloying elements interferes with grain growth during solidification by providing conditions to initiate greater number of nuclei to form, i.e. to promote the formation of finer grains. The solutes form an enriched boundary layer ahead of solidification front in which the actual temperature is lower than that of solidification temperature, constitutional undercooling [2]. The constitutional undercooling as given in Eq. 1 may be interpreted in terms of *Growth Restriction Factor*, GRF. That is when the solidification is controlled by solutal not thermal diffusion and the degree of partitioning $(C_L^* - C_S^*)$ may be approximated to $C_0(1–k)$ when the solutal undercooling, ΔT_s, is small, i.e. $\Delta T_s << (T_m–T_L)$ where T_m is the melting temperature of pure aluminum and T_L is the liquidus temperature for the alloy of C_0 composition [3]. The presence of solute leads to growth restriction as defined by GRF [4, 5] in Eq. 2. The constitutional undercooling is therefore expressed in terms of growth restriction factor in Eq. 3.

$$\frac{G_L}{R} = -\frac{m_L C_0(1-k)}{D_L k} \tag{1}$$

$$\mathrm{GRF} = m_L(k-1)C_0 \tag{2}$$

$$\frac{G_L}{R} = \frac{\mathrm{GRF}}{D_L k} \tag{3}$$

where G_L is temperature gradient in the liquid (K/m); R is growth rate (m/s); C_0 is initial alloy concentration (wt%); m_L is liquidus slope (dT_L/dC) (K/wt%); k is distribution or partition coefficient; C_L^* and C_S^* is

Dr. Reza Ghomashchi was Former NSERC-ALCAN-UQAC Professor and Chair holder; Now Director, Advanced Materials and Processing Research Institute, (http://www.ampr-institute.com/).
Shahrooz Nafisi is Research fellow, Facility for Electron Microscopy Research, McGill University, Montreal, Canada.

S. Nafisi · R. Ghomashchi (✉)
Advanced Materials and Processing Research Group, University of Quebec, Chicoutimi, Quebec G7H 2B1, Canada
e-mail: reza.ghomashchi@ampr-institute.com

Present Address:
S. Nafisi
Facility for Electron Microscopy Research, McGill University, Montreal, Canada

equilibrium solute concentrations of the liquid and solid at the interface (wt%); D_L is diffusion coefficient in the liquid (m^2/s).

It is therefore concluded that the greater the degree of constitutional undercooling, the more effective the solute would be in restricting the grain growth as GRF is inversely proportional to the growth rate.

It was suggested that the growth restriction factor in an alloy should be the sum of GRFs for each alloying element (with assuming that there is no interaction between the solutes) [6, 7]:

$$\mathrm{GRF}_{\mathrm{total}} = \sum_i m_{L,i}\,(C_{0,i} - C_{L,i}*) \tag{4}$$

Table 1 shows the values of the parameters needed for the calculation of GRF numbers, Eq. 2, for the five important elements usually added to Al-alloys. The largest GRF value belongs to Ti having the highest growth restriction effect on aluminum. However, for Al-alloys where Si concentration is appreciable, such as hypoeutectic Al–Si foundry alloys, the high Si content gives an overall higher GRF number. For example for the alloy of 7% Si and 0.1% Ti, the GRF values are 41.3 and ~22 for silicon and Ti, respectively.

For semi-solid metal (SSM) processing of aluminum alloys, the size and morphology of the primary α-Al particles play an important role on the ability of SSM billets in filling the die cavity during casting and more significantly on the mechanical properties of the finished product. As discussed above, solute elements, especially Ti, restrict α-Al growth, so it is expected to achieve smaller globules within the final structure.

For SSM processing, the effect of titanium as grain refiner was studied mainly during the post thermal treatment of grain refined and conventionally cast billets. Most of the previous SSM studies were concentrated on the thixoforming of the pre-refined billets [9–13]. In these methods, globular SSM slurries were prepared by simply reheating grain refined billets. It was reported that the optimum flow behavior for SSM processing is achieved if the microstructure of the raw material consists of very fine and rounded globular grains [10].

In the current study, the effect of dissolved Ti on the morphological changes of primary α-Al particles is investigated for both conventional and SSM castings.

Experimental procedures

The chemical compositions of different 356 alloys used in this study are given in Table 2; it has to be emphasized that the main difference between the alloys is the Ti content. The prepared ingots were melted in a silicon carbide crucible in an electric resistant furnace and degassed by pure argon between 680 and 700 °C.

For conventional casting, the degassed alloy was poured into a graphite cup of 25 mm inside diameter and 5 mm wall thickness which was immersed in the melt for approximately 1 min before sampling to reach the same temperature as the melt. Two K-type thermocouples were quickly immersed into the center and near the wall of the graphite cup containing ~50 g of the alloy. Temperature readings were collected by a National Instrument data logging system at a sampling rate of 10 per second. For these series of experiments, the cooling rates above the liquidus temperature were between 1.5 and 2 °C s^{-1}. The analysis of the cooling curves including the measurement of the critical temperatures was carried out according to the procedure used for determining the solidification temperatures of Al–Si alloys [14]. The following points, were identified and measured on the cooling curves:

- $T_{\mathrm{nuc_{Al}}}$: Start of primary α-Al dendrites nucleation
- $T_{\mathrm{min_{Al}}}$: Unsteady state growth temperature, the temperature beyond which the newly nucleated crystals grow to such extent that the latent heat liberated surpasses the heat extracted from the sample.

Table 1 Data required for calculating the growth restriction factor, GRF [5–8]

Element	k	m_L	$(k–1)m_L$	Max C_0 (wt%)	System
Ti*	7.8, 9	30.7, 33.3	220, 245.6	0.15	Peritectic
Si	0.11	–6.6	5.9	12.6	Eutectic
Mg	0.51	–6.2	3.0	34.0	Eutectic
Fe	0.02	–3	2.9	1.8	Eutectic
Mn	0.94	–1.6	0.1	1.9	Eutectic

*Depend on the reference

Table 2 Chemical analysis of the 356 melts (wt. %)

	Si	Mg	Fe	Mn	Cu	Ti	B	Al
356 without T	6.5–6.8	0.35–0.39	0.07–0.08	0.002–0.012	0.001	Max 0.0058	Nil	Bal.
356 with T	6.5–6.8	0.35–0.39	0.07–0.08	0.002–0.012	0.001	0.1–0.13	Nil	Bal.

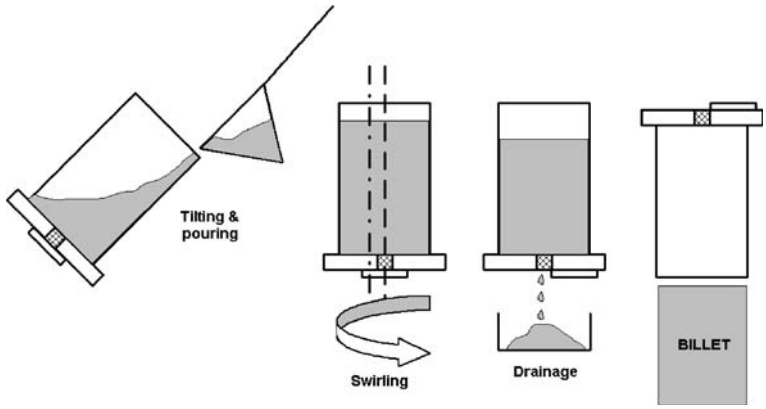

Fig. 1 Schematic representation of the SEED process

- $T_{g_{Al}}$: Steady state growth temperature due to release of latent heat of primary α-Al dendrites
- ΔT_{Rec}: Temperature difference between unsteady ($T_{min_{Al}}$) and steady ($T_{g_{Al}}$) states growth temperatures of the primary α-Al particles (recalescence)

In addition to conventional casting, a new rheocast process, ''Swirled Enthalpy Equilibration Device'', the SEED technology, was used [15]. For the SEED process (Fig. 1), about 2 kg of the alloy was poured at 645 °C into a coated cylindrical steel mold of about 75 mm diameter and 250 mm long. The mold was initially swirled, (off-center), at 2.5 Hz for a certain duration of time to form approximately 0.2–0.3 fraction solid. After that, the bottom enclosure of the mold was opened and the remaining liquid drained for a specific period of time. The overall casting procedure did not exceed more than ~90 s. After draining, the billet was quenched into the cold water. The quenching temperature was 598 ± 2 °C. The cooling rate for this mold and process was approximately 5 °C s^{-1}.

In order to examine the rheological behavior of the billets, several semi-solid slugs were taken out of the mold at the end of the SEED process, i.e. after the drainage of the remaining molten metal, and compressed uniaxially in a simple parallel plate compression machine. The 2.2 kg dead weight applied by a pneumatic lifting system. The press is instrumented to register the applied load and resulting displacement. A cylindrical furnace with two K-type thermocouples installed on the press bed maintains a constant temperature for the billet during the compression tests. The furnace temperature was the same as the billet temperature at the end of casting (598 ± 2 °C). The overall time for rheological tests was ~10 min after which the compressed billets were quenched in water. More information on the in-house constructed parallel plate compression test machine is given elsewhere [16].

Metallographic specimens were prepared by sectioning the conventional graphite mold and SEED billets transversely at the tip of the thermocouples, i.e. 10 and 80 mm from the bottom respectively, and the area between the wall and center was scanned for quantitative microstructural analysis. All specimens were mounted in bakelite, ground, and finally polished down to 0.05 μm diamond paste. For grain size measurements, the linear intercept method was carried out on the anodized specimens.

Image analysis was carried out to characterize the resulting microstructure in the rheocast billets by measuring the number of primary α-Al particles per unit area, i.e. number density, its average circular diameter, aspect ratio (longest/shortest feret diameters), sphericity[1], and area to perimeter ratio, A/P (which is proportional to the inverse of surface area per unit volume [2], S_v). For image processing, a total number of 85 randomly selected fields were analyzed using the automatic stage with the total scanned area of 255 mm^2 per specimen.

Results and discussion

Conventional casting

Thermal analysis

Figure 2 illustrates the effect of dissolved Ti on the early stages of solidification for 2 different Ti concentrations in 356 alloys. The solidification event, nucleation and growth of the primary particles, has been shifted to higher temperature with increasing titanium addition. This is also predictable by thermodynamic calculations. Thermo-Calc[3] software was employed to

[1] Sphericity $= \frac{4\pi A}{P^2}$ where A is total area of primary particles and P is perimeter of liquid–solid interface. The closer the sphericity to one, the higher is the globularity of the particle.

[2] $S_V = \frac{4}{\pi}\frac{P}{A}$

[3] Commercial software for calculation of equilibria, thermodynamic properties and phase diagrams http://www.thermo-calc.com

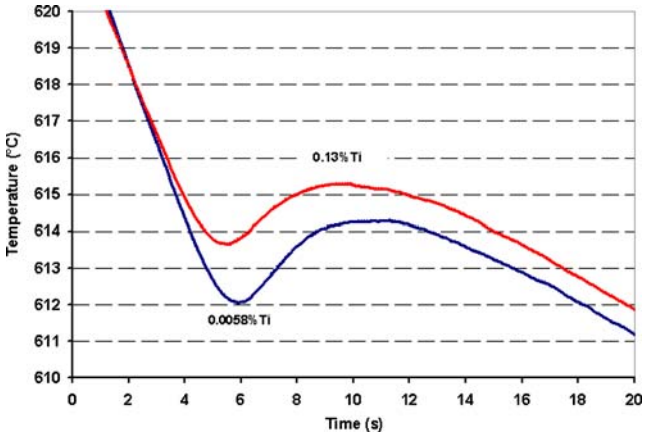

Fig. 2 Typical cooling curves for a selection of samples (central thermocouple) of 356 alloys with different Ti levels

generate pseudo-binary phase diagram, isopleth, for approximately the same alloy composition (Fig. 3), to confirm that the liquidus temperature is ~ 611 °C for this alloy and increases with Ti. The solubility limit for Ti is also ~ 0.12%wt.

Figure 4 shows nucleation ($T_{\mathrm{nuc_{Al}}}$) and recalescence temperatures of the primary α-Al particles. The concept of increasing the liquidus temperature due to Ti addition could easily be seen in Fig. 4 where $T_{\mathrm{nuc_{Al}}}$ is increased by 2–3 °C to about 617 °C. The predicted rise as shown by Thermo-Calc calculation in Fig. 3 is lower. It has to be emphasized that such discrepancies between the predicted and experimental results (Figs. 2–4), are purely attributed to Thermo-Calc calculation being under equilibrium condition while the current study is under non-equilibrium condition including higher cooling rate and presence of other alloying or trace elements.

The solidification recalescence is also decreased by ~1 °C with Ti addition which means there is less growth of the nuclei with smaller recalescence. Bearing in mind that this is a localized region near the tip of thermocouple and with extending this logic across the bulk liquid, it is true to assume growth restriction is effective and the formation of a refined structure should be expected.

Microstructure

Figure 5 shows the microstructural differences between the 0.0058% and 0.13% Ti-containing alloys. The alloy with 0.13% Ti has finer dendritic structure, and the grain size appears to have been reduced considerably, see the polarized light photomicrographs in Fig. 5.

It may be argued that such refinement is due to more effective nucleation, not the growth restriction capability of Ti. In order to clarify this issue, it is helpful to define the two concepts of ''grain refining'' and ''grain growth restriction''. The former is dependent primarily on the presence and then the size, population and morphology of nucleants, i.e. independent Ti-based compounds, while the latter is about the dissolved Ti in the α-Al matrix and its diffusion across solid–liquid interface. It is believed at this level of Ti concentration, it is rather unlikely and remote to have independent Ti-based particles, since as shown in Fig. 3, the formation of Ti-based compounds, i.e. the potential nucleants,

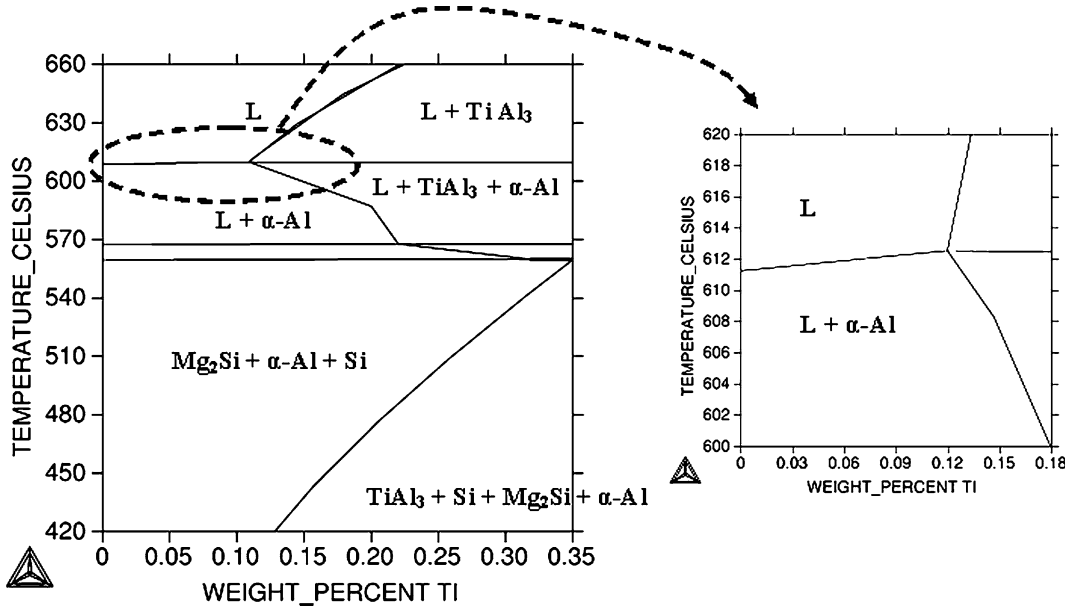

Fig. 3 Thermo-Calc calculated pseudo-binary phase diagram, isopleth, for Al7Si1Mg with increasing Ti

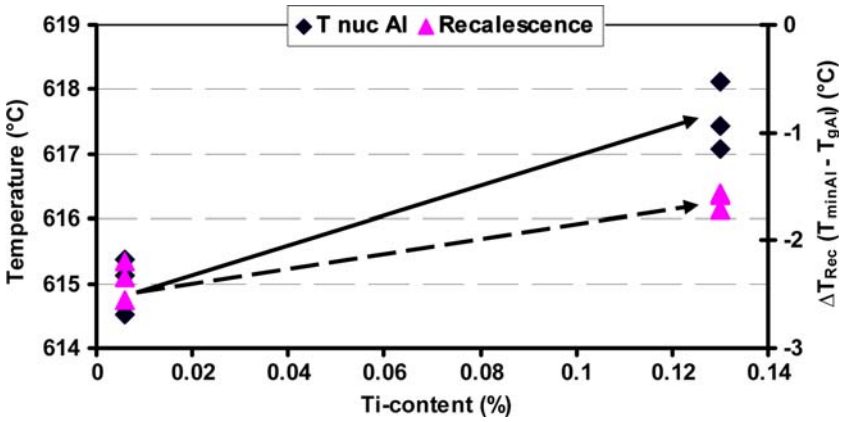

Fig. 4 The effect of dissolved Ti on the nucleation temperature and ΔT_{Rec} (undercooling) of the primary α-Al particles

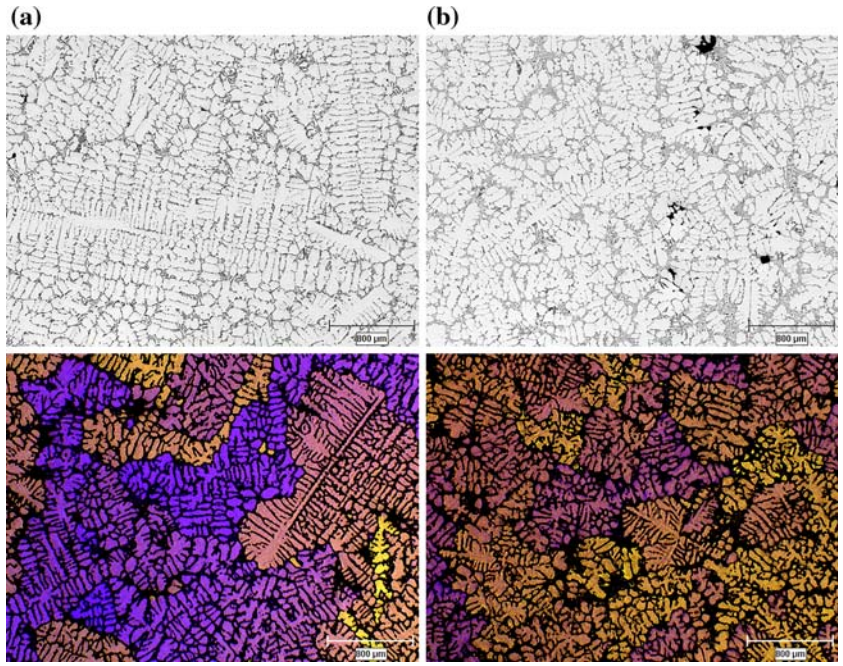

Fig. 5 The effect of dissolved Ti on the microstructure of the 356 Al–Si alloys: (**a**) with 0.0058% Ti, (**b**) 0.13%Ti

only begin at Ti% > 0.12. Therefore, the concerning issue should be the diffusion of Ti at the solidification interface and its rate controlling role on the primary α-Al growth. The growth restriction concept is thus more acceptable than the formation of Ti-based nucleants to render more effective nucleation, especially at the early stages of solidification. However, it may be true to assume that such diffusion of Ti may eventually lead, in a localized volume, to the formation of Ti-based nucleants, but this is a far-distant time event and surely not at the beginning of solidification, i.e. the diffusion of Ti is a pre-requisite for such mechanism.

Figure 6 shows the effect of Ti on the grain size of 356 alloys. For the alloy with 0.0058%Ti in solution, the average grain size is about 1100 μm and reduces to around 850 μm when Ti concentration is increased to 0.13%, a grain size reduction of almost 22%. Furthermore, the value of standard deviation is much greater for the alloy with lower Ti-content which is a clear indication of wider distribution of grain size in this alloy. For higher Ti-content, the smaller value of standard deviation suggests a more uniform grain size, and consequently the properties are expected to be much more uniform.

It is further clear from Fig. 6 that the grain size and nucleation temperature of the primary α-Al particles vary inversely with increasing Ti in solution; the average α-Al grain size decreased with increasing nucleation temperature. The rise in nucleation temperature is simply to extend the nucleation period and generate more nuclei. It must be emphasized that the rate of nucleation does not change, since the energy barrier of the system for nucleation should remain the same during the early stages of solidification.

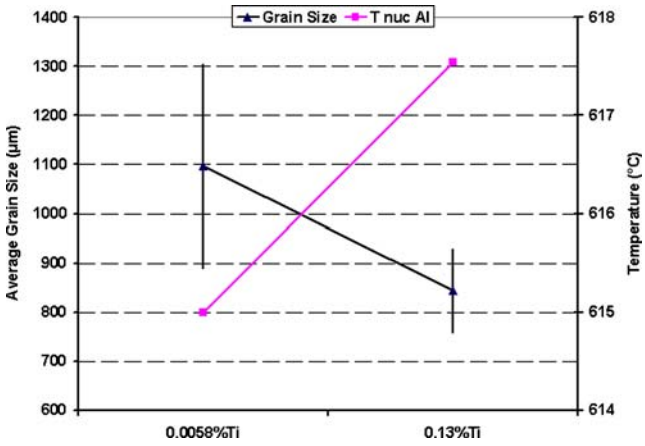

Fig. 6 Relation between grain size and $T_{\mathrm{nuc_{Al}}}$ in different Ti content

Backerud and Johnsson [7] conducted a series of experiments on the grain refining efficiency for Al–Si system and their results are presented in Fig. 7. Figure 7a shows that the concentration of dissolved Ti in promoting a fine structure is only effective at lower concentrations of Si, below 2–3%, where increasing Ti content has a positive effect in reducing the grain size, but becomes impotent with increasing Si. In other words, the coarsening effect of Si completely nullifies growth restriction capabilities of dissolved Ti.

The strong effect of Si in promoting grain coarsening is illustrated in their conclusion on the interrelationship of grain size and the total GRF number in Fig. 7b. As seen, the data for alloys similar to that of the current study and most of the commercial Al–Si alloys are mainly located on the right hand side of the graph, which means the grain size should increase with increasing GRF value. In other words the grain size should increase with increasing Ti concentration in solution. The current results support the opposite, where the grain size decreased with higher percentages of Ti in solution. Such discrepancy was also reported by Pasciak and Sigworth [17]. It appears that the correlation between grain size and total GRF value needs further clarification.

Rheocasting

Microstructure

The optical micrographs in Fig. 8 show the resulting microstructure in the SEED billets. The primary α-Al particles are almost fully globular irrespective of the Ti content. The fine eutectic structure in both micrographs is due to the quenching of the billets in cold water which also prevented further coarsening of the primary α-Al particles.

Although the microstructure of the alloy containing 0.13% Ti appears to have been slightly refined (Fig. 8) the effect of dissolved Ti on the microstructure is better realized if it is characterized quantitatively. Therefore, both quantitative metallography and rheological tests were carried out on different Ti-containing alloys to highlight grain growth restriction, and the results are discussed later in this report (see Figs. 9, 10, 11).

The concept of structural refining with dissolved Ti may be explained with reference to constitutional supercooling where the growing primary α-Al dendrites reject Ti into the solid–liquid interface as they grow. The rejected Ti atoms build up ahead of the solidification interface and form a Ti-enriched boundary layer. This is graphically illustrated in Fig. 9 where the concentration of Ti at the boundary layer varies for different Ti concentrations due to differences in the diffusion fluxes for various Ti contents. The value of diffusion flux (J), $J = -DA(\partial c/\partial x)$ is greater for 0.13%Ti than that of 0.0058, since $(\partial c/\partial x)$, is greater for 0.13% Ti. Therefore, the degree of constitutional supercooling is much greater for 0.13% Ti than that of

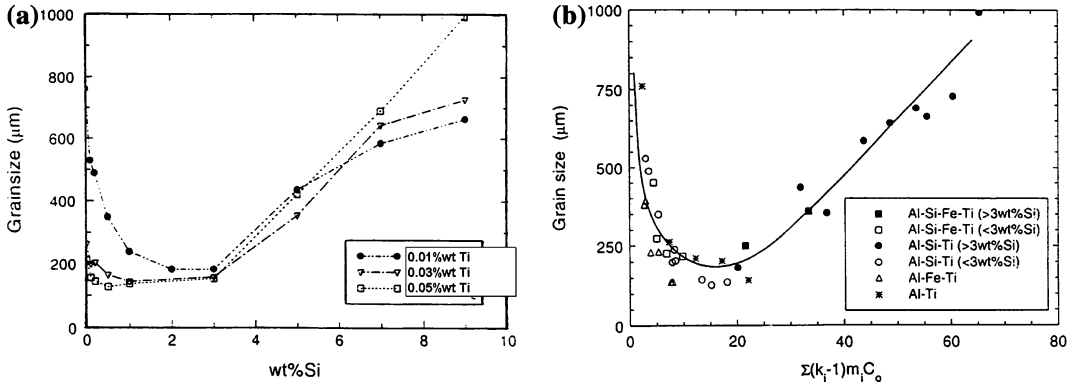

Fig. 7 (**a**) grain size variation according to Si and Ti content in Al–Si alloys solidified at 1°C s^{-1}, (**b**) the effect of GRF values on the average grain size for a number of alloy compositions [17]

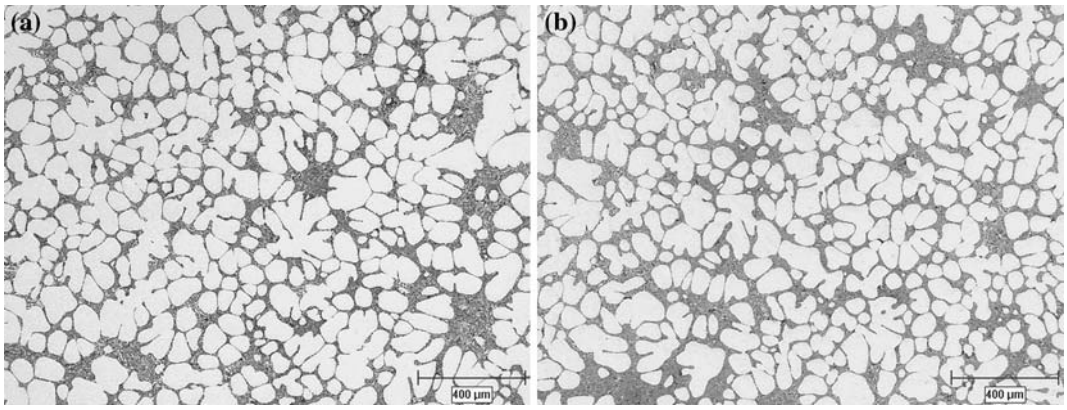

Fig. 8 Optical micrographs in the SEED process: (**a**) 0.0058%Ti, (**b**) 0.13%Ti

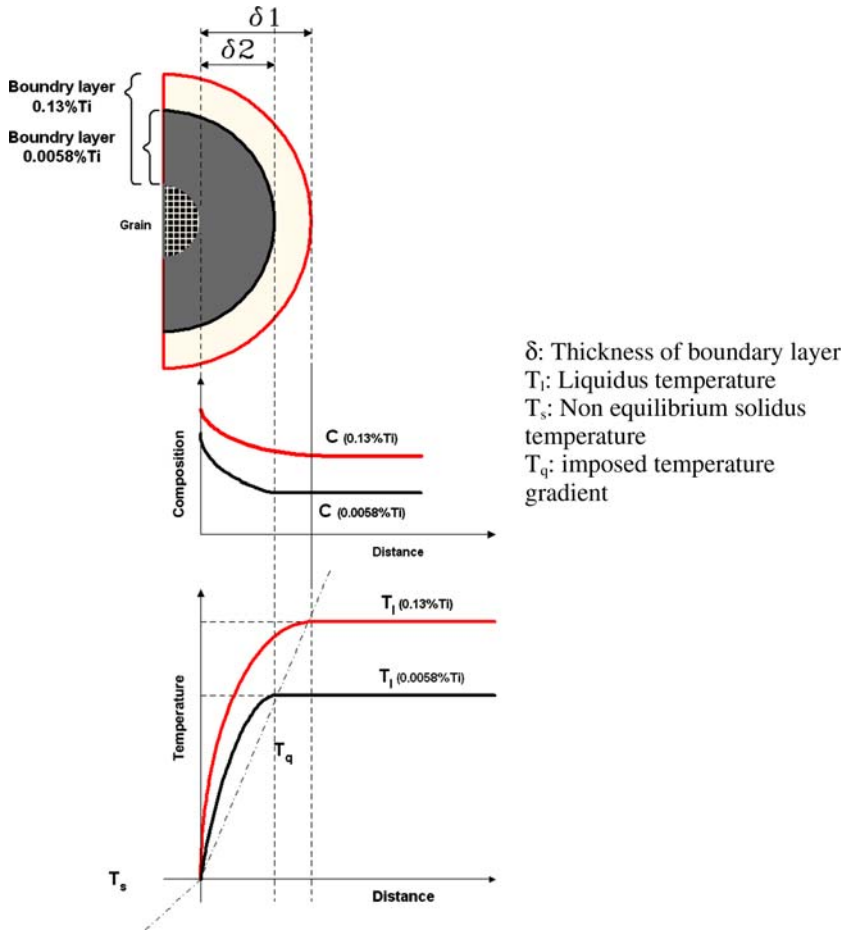

Fig. 9 Schematic of constitutional supercooling in different solute buildup

0.0058% Ti. Equally, the boundary layer thickness is greater for higher Ti content alloy as schematically illustrated in Fig. 9. As pointed out by Kurz and Fisher [18], the equivalent boundary layer thickness (δ_c) is inversely proportional to growth rate, (V), for an alloy solidified at different growth rates, as given in Eq. 5;

$$\delta_c = \frac{2D}{V} \tag{5}$$

where D is the diffusion coefficient for dissolved titanium. Since higher growth rates are equivalent to lesser diffusion and rejection of solute element into the boundary layer, i.e. lower $\frac{\partial c}{\partial t}$, it may be acceptable to consider higher concentration of solute element within the boundary layer is equivalent to that of lower growth velocity or greater thickness of this layer. This is indeed the concept of growth restriction discussed in the previous paragraph.

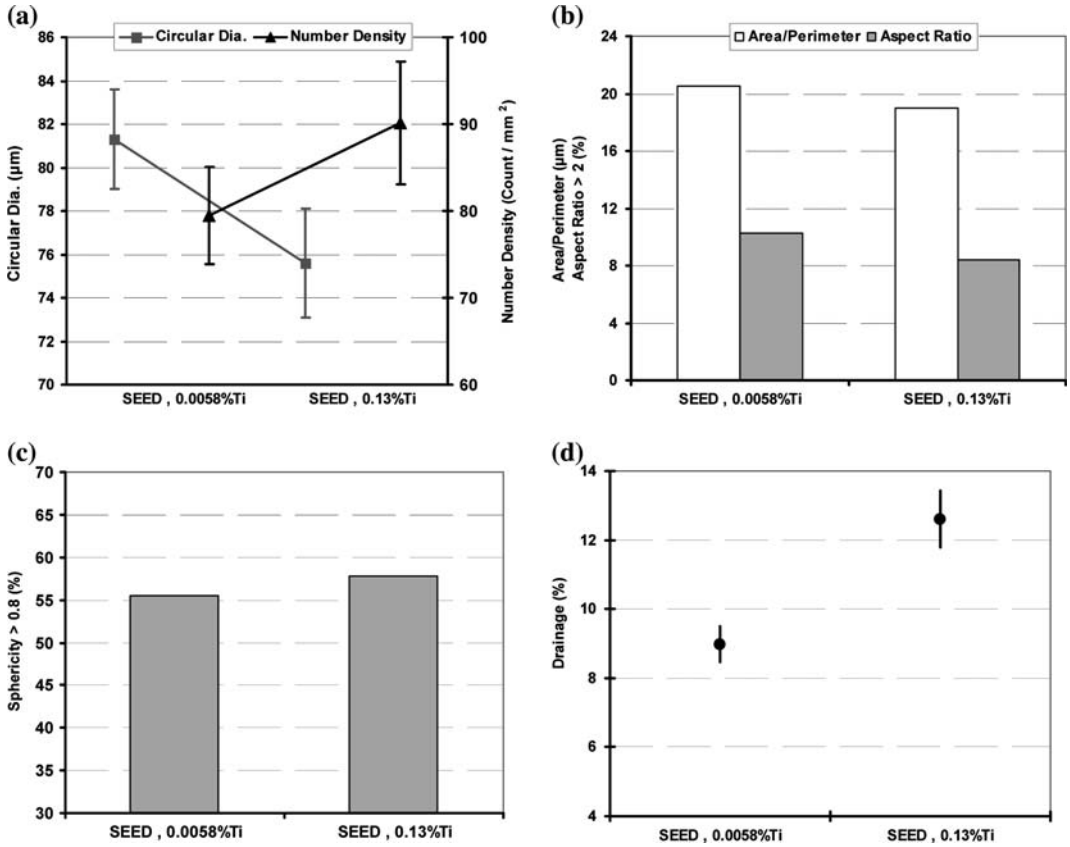

Fig. 10 Image analysis parameters for 356 alloys: (**a**) circular diameter and number density of α-Al particles, (**b**) area/perimeter and percentage of particles having aspect ratio > 2 , (**c**) the percentage of particles having sphericity > 0.8, and (**d**) drainage percentage of the remaining liquid

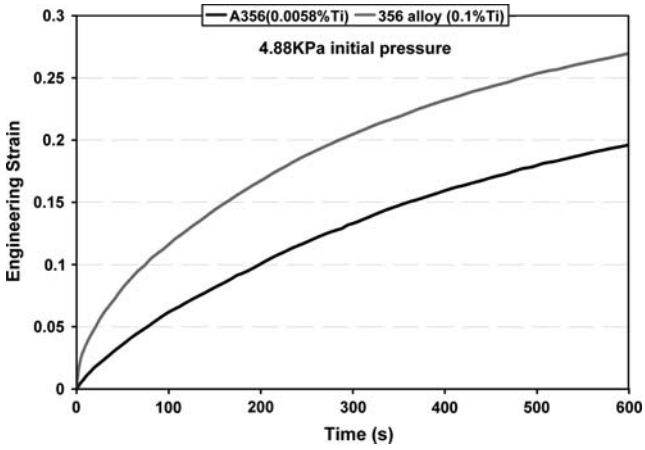

Fig. 11 Strain–time graphs for different Ti in solution

Furthermore, as the concentration of Ti increases at the interface during later stages of solidification, it may reach the level where new nucleants of Al_3Ti could form within the interface layer. The presence of such particles encourages the formation of new α-Al nuclei within the interface. The newly formed α-Al particles are expected to reject Ti into the newly formed interfaces as they grow. The repetition of such mechanism ensures the formation of finer and more equiaxed and spherical particles as observed in 0.13%Ti added 356 alloy (Figs. 5, 8).

The results of quantitative metallography are presented in Fig. 10. The mean globule size, equivalent circular diameter, appears to have decreased with increasing Ti content. Nevertheless, the globule size was always less than 100 μm regardless of Ti concentration which is an indication of the process capability in producing high quality rheocast billets [19].

The rise in the number of α-Al particles per unit area (mm^2), number density, coupled with the reduction of area to perimeter ratio, *A/P*, indicate microstructural refinement leading to the formation of more isolated and finer particles in the Ti-content billets.

From solidification point of view, with the addition of growth restricting elements such as Ti, dendrite growth tends to slow down in direction opposite to heat flow approaching those of the lateral growth. The overall growth therefore tends to be more radial and

the resulting structure should be more globular. The formation of spheroidal particles are critical on the rheological behavior of the slurries as discussed later in this article. This is clearly shown by the reduction in percentage of the primary α-Al particles with aspect ratio greater than 2. The formation of more spherical particles is further supported by the rise in the percentage of particles with sphericity number greater than 0.8 with increasing Ti content (Fig. 10b, c).

As pointed out before, the final stage in the SEED process is draining a portion of the remaining liquid from the system to have a self-standing billet. The quantity of drainage may be regarded as an indication of fluidity in micro scale, micro-fluidity. It has to be emphasized that this may be contradictory to the classical meaning of fluidity which is normally defined as the distance to which a metal will run before solidification. That is why the concept of ''micro-fluidity'' is employed, ''the flow of molten alloy through a network of primary α-Al particles''.

Figure 10d illustrates more drainage of the remaining liquid with higher Ti in solution. This may be due to the formation of spherical particles within alloy having higher Ti and thus the ease of liquid flow through the less complex inter-particle channels. This concept could be compared to that of the Dendrite Coherency Point[4] (DCP) in the conventional casting and the fact that mass flow persists further, i.e. postponement of DCP to lower temperatures, with grain refining [20].

Strain–time graphs

The effect of α-Al morphology on the ability of billets to deform is clearly detectable in the strain–time graphs presented in Fig. 11. Three distinct regions may be recognized on these graphs as reported before [16, 21]:

1. Stage I, where the billet flows almost without any resistance to applied pressure. It may be attributed to easy movement of the primary α-Al particles within the residual liquid and without appreciable collision. The extent of this region is dependent on the degree of globularity of the primary α-Al particles.

This is in agreement with Chen et al. results [22] where they proposed lateral liquid flow coupled with solid particles movement towards each other in the vertical direction as the main cause of easy flow during step-I. They also pointed out that step-I brings about solid/liquid segregation within the deformed billet.

As it is evident, the extent of this region appears to be dependent on Ti concentration where less resistance to deformation is shown for higher Ti content.

2. Stage II, where there is some degree of resistance to flow. This is due to the collision of solid particles and formation of α-Al agglomerates. The agglomerated chunks are the resisting constituents to billet flow.

This is also similar to what has been reported by Chen et al., where cooperative movement of solid and liquid phases is responsible for billet deformation. This is accompanied by some degree of resistance to flow where solid particles not only move vertically but also laterally. For constant force, the slope of the curve should decrease due to this resistance. As for the stage I, the ability of billets to deform increases with increasing Ti content.

Both stages I and II are regarded as non-steady state, since the slope of the graphs vary with time. The reducing trend in the slope may be attributed to mainly the collision and agglomeration of the primary α-Al particles.

3. Stage III, where the billet flows almost steadily with a constant slope. It is believed the two processes of agglomeration and de-agglomeration have reached an equilibrium state, i.e. quasi steady state equilibrium.

This is the stage where the authors believe has been neglected by Chen et al. [22]. They have defined step III as the section that the deformation force increases sharply since it should overcome the friction generated from the sliding between solid particles and also affecting by surrounding particles. This is believed to be stage IV according to the current study, where the deformation force for this step should be larger than the last steps.

As for the stages I and II, the ability of billets to deform in stage III increases with increasing Ti content.

The changes in the billets deformability due to the primary α-Al particles size and distribution are clearly detectable on the graphs in Fig. 11. The alloy with almost no Ti shows the lowest strain values while the commercial 356 billet deforms at much higher range due to smaller globule size as already discussed. As reported before [21] the billets with more globular and finer microstructure yield greater engineering strain, i.e. better flow. In other words, the superior flow of the alloy with higher Ti content is due to its structure having more globular and finer grains which enables it to flow better. Furthermore, the parameters from

[4] The temperature at which mass flow of the molten alloy changes to interdendritic flow.

Fig. 10, especially average circular diameter and number density of α-Al particles, clearly support the conclusion that the billet with higher dissolved Ti has more globules with smaller size.

Conclusions

The effect of dissolved Ti to refine Al–Si 356 alloy grain size is highlighted for both conventional and semi solid castings. Primary α-Al nucleation temperature increased by 2–3 °C and solidification undercooling decreased about 1 °C due to minor addition of Ti. For the rheocasting operation, the size of globules decreased and globularity increased by the dissolved Ti. This is equivalent to improved rheological properties especially flow properties which is of great importance during high pressure die casting of semi-solid billets.

Acknowledgements The work reported here is part of an NSERC-Discovery grant and NSERC-ALCAN-UQAC industrial research chair, Grant No. IRCPJ268528-01, on the ''Solidification and Metallurgy of Al-alloys''. The authors would like to gratefully acknowledge financial support from Natural Sciences and Engineering Research Council of Canada, ALCAN International Limited, Centre Québécois de recherche et de développement de l'aluminium (CQRDA), la Fondation de l'UQAC and the endowment fund of UQAC. Joseph Langlais of ALCAN-ARDC, for his continued interest, and Omid Lashkari of our research group, for carrying out the rheological tests, are gratefully acknowledged.

References

1. Kissling RJ, Wallace JF (1963) Foundry(June) 78
2. Chalmers B (1964) Principles of solidification. John Wiley & Sons Inc, New York
3. Quested TE, Dinsdale AT, Greer AL (2005). Acta Mater 53:1323
4. Maxwell I, Hellawell A (1975) ACTA Metal 23:229–237
5. Johnsson M, Backerud L (1996) Metallkde Z 87:216–220
6. McCartney DG (1989). Int Mater Rev 34(5):247–260
7. Backerud L, Johnsson M (1996) TMS Light Metals 679
8. Easton MA, StJohn DH (2001) Acta Mater 49:1867–1878
9. Wan G, Witulski T, Hirt G (1993) In: Thixoforming of Al alloys using modified chemical grain refinement for billet production – Conference on aluminum alloys: New Process Technologies, Italy, June 1993. pp 129–141
10. Gabathuler JP, Barras D, Krahenbuhl Y (1992) Evaluation of various processes for the production of billet with thixotropic properties. 2nd international conference on semi-solid processing of alloys and composites. MIT, Cambridge, USA, pp 33–46
11. Mertens HP, Kopp R, Bremer T, Neudenberger D, Hirt G, Witulski T, Ward P, Kirkwood DH (1997) Comparison of different feedstock materials for thixocasting. EUROMAT 97, Proceedings of the 5th European conference on advanced materials and processes and applications. pp 439–444
12. Bergsma SC, Tolle MC, Kassner ME, Li X, Evangelista E (1997) Mater Sci Eng A237: 24
13. Brusethaug S, Voje J (2002) Manufacturing of feedstock for semi-solid processing by chemical grain refinement. 6th international conference on semi-solid processing of alloys and composites, Turin, Italy. pp 451–456
14. Backerud L, Chai G, Tamminen J (1990) Solidification characteristics of aluminum alloys, Vol 2, foundry alloys. American Foundry Society Inc, Des Plaines, IL
15. Doutre D, Hay G, Wales (2002) United States Patent No. 6428636, Aug 6, 2002
16. Lashkari O, Ghomashchi R, Adjersch F (2005) In: Schlesinger ME (ed) Rheological study of 356 Al–Si foundry alloy prepared by a new innovative SSM process. Extraction and Processing Division (EPD), TMS publication, San Francisco, pp 149–156
17. Pasciak KJ, Sigworth GK (2001) AFS Trans 109
18. Kurz W, Fisher DJ (1989) Fundamental of solidification. Trans Tech Publication, Switzerland
19. Apelian D (2002) Semi-solid processing routes and microstructure evolution, 7th international conference on semi-solid processing of alloys and composites, Tsukuba, Japan, 2002. pp 25–30
20. Chai G, Rolland T, Arnberg L, Backerud L (1992) Studies of dendrite coherency in solidifying aluminum alloy melts by rheological measurements. 2nd international conference on semi-solid processing of alloys and composites, Cambridge, MA. pp 193–201
21. Lashkari O, Ghomashchi R (2006) The implication of rheological principles for characterization of semi-solid Al–Si cast billets. J Mat Sci (in press)
22. Chen CP, Tsao CYA (1997) Acta Metal 45(5):1955